Full title

Exploring the Complexity of Protein-Level Dosage Compensation that Fine-Tunes Stoichiometry of Multiprotein Complexes

Short title

Dosage Compensation and Stoichiometry of Multiprotein Complexes

Author names and affiliations

Koji Ishikawa[1,*,#a], Akari Ishihara[2], Hisao Moriya[1,2]
[1] Research Core for Interdisciplinary Sciences, Okayama University, Okayama 700-8530, Japan
[2] Course of Agrochemical Bioscience, Faculty of Agriculture, Okayama University, Okayama 700-8530, Japan
[#a] Current Address: The Center for Molecular Biology, ZMBH-DKFZ Alliance, Heidelberg University, Im Neuenheimer Feld 282, D-69120 Heidelberg, Germany

[*] Correspondence: k.ishikawa@zmbh.uni-heidelberg.de

Abstract

Proper control of gene expression levels upon various perturbations is a fundamental aspect of cellular robustness. Protein-level dosage compensation is one mechanism buffering perturbations to stoichiometry of multiprotein complexes through accelerated proteolysis of unassembled subunits. Although N-terminal acetylation- and ubiquitin-mediated proteasomal degradation by the Ac/N-end rule pathway enables selective compensation of excess subunits, it is unclear how dominant this pathway contributes to stoichiometry control. Here we report that dosage compensation depends only partially on the Ac/N-end rule pathway. Our analysis of genetic interactions between 18 subunits and 10 quality control factors in budding yeast demonstrated that multiple E3 ubiquitin ligases and N-acetyltransferases are involved in dosage compensation. We find that N-acetyltransferases-mediated compensation is not simply predictable from N-terminal sequence despite their sequence specificity for N-acetylation. We also find that the compensation of Pop3 and Bet4 is due in large part to a minor N-acetyltransferase NatD. Furthermore, canonical NatD substrates histone H2A/H4 were compensated even in its absence, suggesting N-acetylation-independent compensation. Our study reveals the complexity and robustness of the stoichiometry control system.

Author Summary

Quality control of multiprotein complexes is important for maintaining homeostasis in cellular systems that are based on functional complexes. Proper stoichiometry of multiprotein complexes is achieved by the balance between protein synthesis and degradation. Recent studies showed that translation efficiency tends to scale with stoichiometry of their subunits. On the other hand, although protein N-terminal acetylation- and ubiquitin-mediated proteolysis pathway is involved in selective degradation of excess subunits, it is unclear how dominant this pathway contributes to stoichiometry control due to the lack of a systematic investigation using endogenous proteins. To better understand the landscape of the stoichiometry control system, we examined genetic interactions between 18 subunits and 10 quality control factors (E3 ubiquitin ligases and N-acetyltransferases), in total 100 combinations. Our data suggest that N-acetyltransferases are partially responsible for stoichiometry control and that N-acetylation-independent pathway is also involved in selective degradation of excess subunits. Therefore, this study reveals the complexity and robustness of the stoichiometry control system. Further dissection of this complexity will help to understand the mechanisms buffering gene expression perturbations and shaping proteome stoichiometry.

Introduction

Controlling intracellular protein concentration at the proper level is a critical aspect of cellular systems. For example, it has been suggested that the cells regulate proteome concentration for a constant rate of biochemical reactions [1-3]. Moreover, since a wide variety of stress response pathways dynamically change the expression of proteins responsible for survival in various challenging environments, it is obvious that the control of protein concentration is also important for coping with perturbations and maintaining cellular homeostasis.

Genome-wide studies measuring cellular robustness against genetic perturbations showed that *Saccharomyces cerevisiae* cells are fragile against protein overexpression of a subset of the genome [4, 5]. This finding indicates that the cell system is generally robust against genetic perturbations to various biological processes. However, it is unclear how cells buffer such environmental changes [6]. We recently reported that upon an increase in gene copy number, approximately 10% of the yeast genome are transcribed linearly into mRNA levels but not directly translated into protein levels [7]. Comprehensive analyses of aneuploid yeast and mammalian cells also showed that approximately 20% of the genome exhibit this molecular phenotype [8, 9]. Therefore, this phenomenon known as protein-level dosage compensation may partially explain the buffering of gene expression perturbations.

Protein-level dosage compensation predominantly targets genes encoding subunits of multiprotein complexes [7-10]. The concentration of the dosage-compensated proteins bidirectionally changes in response to that of its partner subunits [7, 11]. These observations are consistent with a hypothesis predicting the deleterious effects due to stoichiometric imbalance of the complex subunits on cell growth [5, 6, 12]. Another line of evidence for this prediction comes from ribosome profiling analyses revealing a proportional synthesis strategy that enables translation efficiency to scale with subunit stoichiometry [13, 14]. This finding shows that stoichiometric balance of multiprotein complex subunits is mainly maintained at the translational level. In addition, this strategy is conserved from bacteria to higher eukaryotes [14]. In this context, dosage compensation can be recognized as a fail-safe mechanism that fine-tunes proteome stoichiometry [15].

The mechanism of dosage compensation is accelerated degradation of unassembled subunits by the ubiquitin–proteasome system [7, 11, 16, 17]. Multiple E3 ubiquitin ligases involved in stoichiometry control were previously identified [11, 18, 19], but we lack an understanding of their relative contribution to the compensation of identical subunits [20]. Furthermore, the underlying mechanism for selective degradation of excess subunits is not well understood. Although previous studies found evidence for selective compensation of Cog1 and Hcn1 in yeast and PLIN2 in mammalian cells by the Ac/N-end rule pathway [11, 21], it is unclear how dominant this pathway contributes to the compensation. The Ac/N-end rule pathway is one mechanism for protein degradation through the acetylation of N-terminal amino acid by N-acetyltransferases (NATs). With the limited number of examples, N-acetylation was shown to act as a degradation signal (N-degron) recognized by specific E3 ubiquitin ligases (N-recognin) [11, 18, 22]. It has been hypothesized that N-degron of unassembled subunit is exposed and recognized by N-recognin, whereas that of assembled subunit is shielded by the other subunits in the same complex and is inaccessible by N-recognin (Fig 1A) [11, 18, 23]. This model is consistent with the biological role of dosage compensation, but it remains to be investigated whether the compensation depends on this pathway.

In this study, we measured the contribution of E3 ubiquitin ligases and NATs to dosage

110 compensation of the RNase P/MRP subunits, which are the compensated proteins identified
111 in our previous study [7], in a systematic manner. We find that multiple E3 ubiquitin ligases
112 and NATs are involved in the compensation. We also find that the dependency of the com-
113 pensation on NATs is variable among tested subunits. Our findings suggest that dosage com-
114 pensation does not completely depend on the Ac/N-end rule pathway and highlight the com-
115 plexity of the stoichiometry control system.

Results

Multiple E3 ubiquitin ligases Tom1 and Not4 are involved in dosage compensation of identical subunits

To investigate which E3 ubiquitin ligases are involved in dosage compensation and their relative contribution, we measured protein levels of five dosage-compensated genes (*RBG1*, *MTW1*, *POP5*, *SAW1*, and *ERP2*), which were identified in our previous study [7], in five deletion mutants of E3 genes (*DOA10*, *TOM1*, *UBR1*, *SAN1*, and *NOT4*) involved in the protein quality control system including the N-end rule pathways [11, 18, 19, 24, 25]. Using a previously developed method for identifying genes with dosage compensation (S1A Fig) [7], we found that the amount of Pop5 in *tom1*Δ and *not4*Δ and Saw1 in *doa10*Δ was increased compared to wild type (WT) cells (S1B and S1C Fig).

Pop5 is a subunit of the RNase P/MRP complexes comprising of eleven subunits [26]. These complexes share eight subunits: Pop1, Pop3, Pop4, Pop5, Pop6, Pop7, Pop8, and Rpp1, while Rpr2 is included only in the RNase P and Snm1 and Rmp1 are included only in the RNase MRP. Most subunits of these complexes are subjected to dosage compensation [7], which prompted us to examine whether Tom1 and Not4 are involved in the compensation of the other subunits. We used an experimental setup by which the TAP-tagged target protein expressed from only one genomic locus is detected upon an increase in copy number of untagged version of the same gene (Fig 1B). We first compared protein levels between with and without overexpression in WT, *tom1*Δ, or *not4*Δ cells (S2A Fig). This analysis showed a significant decrease in the compensation of Pop4, Pop5, Pop6, Pop7, Pop8, and Rpp1 in *tom1*Δ cells (Fig 2A and 2B), as well as Pop4, Pop5, Pop7, Rpp1, and Rmp1 in *not4*Δ cells (Fig 2D and 2E). In addition, the lower compensation of Rpr2 and Rmp1 in *tom1*Δ cells were marginally significant ($p<0.1$, two-tailed Welch's *t* test) (S3 Fig). Therefore, Tom1 and Not4 were involved in dosage compensation of the RNase P/MRP subunits: Tom1 and Not4 target at least 6 and 5 out of 11 subunits, respectively (Table 1). While the sum of the contribution of these E3 ligases to the compensation of Pop7, Pop8, and Rpp1 reached to uncompensated protein level (Fig 2G), that of the other subunits did not reach to this level, which suggests the existence of unidentified E3 ligase(s) responsible for stoichiometry control.

We next compared protein levels between WT and each mutant with or without overexpression (S2B Fig). This analysis showed the higher levels of Pop6 and Rpr2 in *tom1*Δ and Pop5 and Pop6 in *not4*Δ than those in WT cells without an increase in gene copy number ($p<0.05$, two-tailed Welch's *t* test) (Fig 2C and 2F, Single). As this comparison is between vector controls in WT and mutant cells, Tom1 and Not4 may be involved in degradation of these subunits in unperturbed conditions. In addition, since Pop6 was not subjected to Not4-mediated compensation, Not4 contributes to its degradation but this is not accelerated upon overexpression.

156 **Figure 1**
157

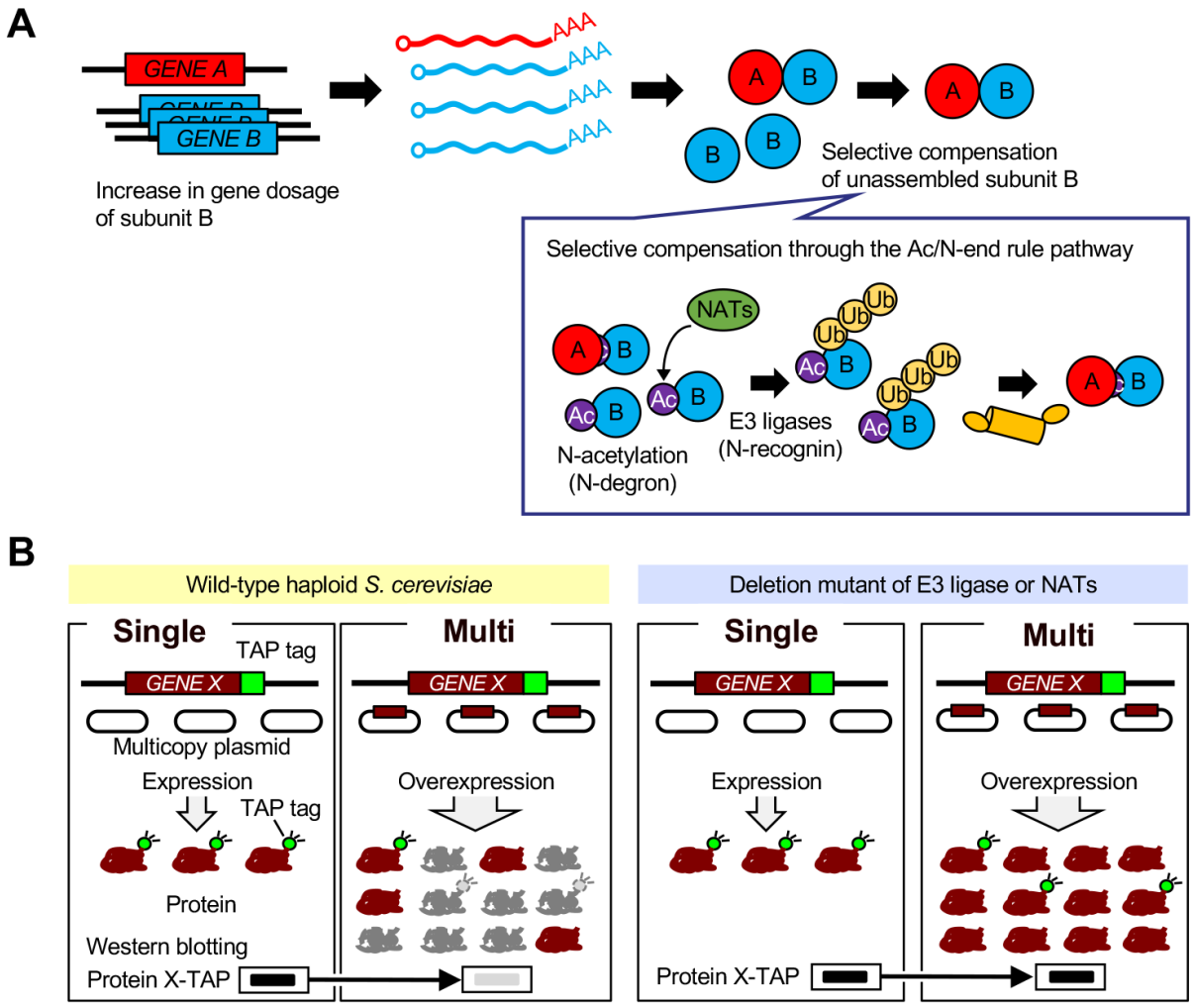

158
159

160 **Fig 1. Genetic perturbation analysis of the stoichiometry control system.**
161 (**A**) Protein-level dosage compensation predominantly targets subunits of multiprotein com-
162 plexes. The Ac/N-end rule pathway is involved in the underlying mechanism for the selective
163 compensation of unassembled subunits. (**B**) An experimental setup for measuring the contri-
164 bution of each quality control factor to dosage compensation. The untagged dos-
165 age-compensated protein was expressed from multicopy plasmid pTOW40836 containing the
166 native regulatory sequences, including promoter and 5' and 3' untranslated regions. If the
167 target gene is subjected to dosage compensation, the level of the TAP-tagged target protein
168 expressed only from the chromosome decreases upon an increase in gene copy number (Mul-
169 ti) compared to vector control (Single). The Multi/Single ratio is higher than that in WT cells
170 in the deletion mutant of each quality control factor (gene encoding E3 ubiquitin ligase or a
171 catalytic subunit of NATs) if the deleted factor contributes to the compensation of the target
172 gene.

173 **Figure 2**
174

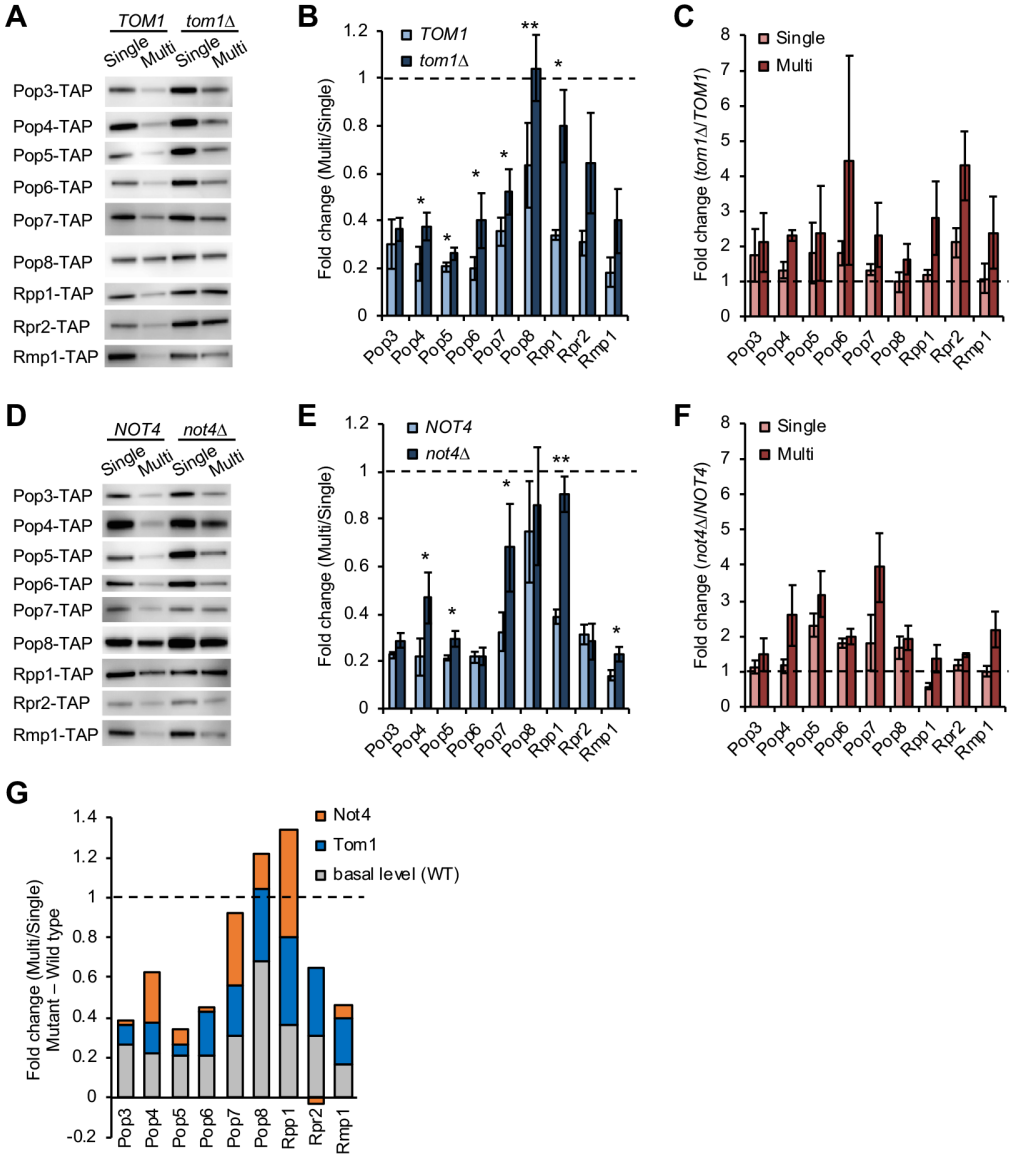

175
176

177 **Fig 2. Tom1 and Not4 are involved in dosage compensation.**
178 (**A**) Western blots of the RNase P/MRP subunits in *tom1*Δ cells. The TAP-tagged subunit ex-
179 pressed from the chromosome was detected with PAP. Pop1 and Snm1 were not detected in
180 our experiments. A representative blot from three biological replicates is shown. (**B**) Quanti-
181 fication of protein levels in the Multi condition relative to those in the Single condition in WT
182 and *tom1*Δ cells. The average fold change ± s.d. was calculated from three biological repli-
183 cates. Statistical significance was determined by a two-tailed Welch's *t* test ($^{*}p<0.05$,
184 $^{**}p<0.01$). Dashed line represents the same expression level between the Single and Multi
185 conditions. (**C**) Comparison of protein levels between WT and *tom1*Δ cells in the Single or
186 Multi conditions. The average fold change ± s.d. was calculated from three biological repli-
187 cates. Dashed line represents the same expression level between WT and *tom1*Δ cells. (**D–F**)
188 Same as in (**A–C**), except that shown are Western blots of the RNase P/MRP subunits in
189 *not4*Δ cells (**D**) and their quantification (**E, F**). (**G**) The relative contribution of Tom1 and
190 Not4 to the compensation. The basal level is the average fold change in WT cells. The con-
191 tribution of Tom1 and Not4 was calculated as the average fold change in each mutant minus
192 the basal level.

Dosage compensation of Pop6 and Pop7 occurs in response to their intracellular concentration

Since both Pop6 and Pop7, which form the Pop6–Pop7 heterodimeric subcomplex [27, 28], are subjected to dosage compensation (Fig 2), the amount of Pop6 and Pop7 may change in response to that of partner subunits. We hypothesized that high *POP7* dosage leads to changes in the fraction of the stable/assembled and unstable/unassembled pools of Pop6 (Fig 3A, top). Furthermore, since the mechanism of dosage compensation is accelerated degradation of unassembled subunits, the balance of these subunit pools may be perturbed in the absence of Tom1 or Not4 (Fig 3B, top). As expected (Fig 3A and 3B, bottom), we found that Pop6 was stabilized by an increase in *POP7* dosage, and vice versa, in WT, *tom1*Δ, or *not4*Δ cells (Fig 3C and 3D). These results indicate that dosage compensation of Pop6 and Pop7 occurs bidirectionally in response to changes in intracellular concentration of each subunit: accelerated degradation of Pop6/Pop7 upon high *POP6*/*POP7* dosage (downward compensation) and reduced degradation of Pop6/Pop7 upon high *POP7*/*POP6* dosage (upward compensation).

Upon increasing gene copy number of the partner subunit, the relative ratio of Pop6 and Pop7 in *tom1*Δ and *not4*Δ was lower than that in WT cells. This difference may reflect the regulation of the compensation degree, as the amount of Pop6 and Pop7 was increased in both mutants without changes in gene copy number (Fig 3C and 3D, +Vector). Therefore, Tom1 and Not4 impact the balance of stable/unstable subunit pools of the Pop6–Pop7 heterodimeric subcomplex.

214 **Figure 3**
215

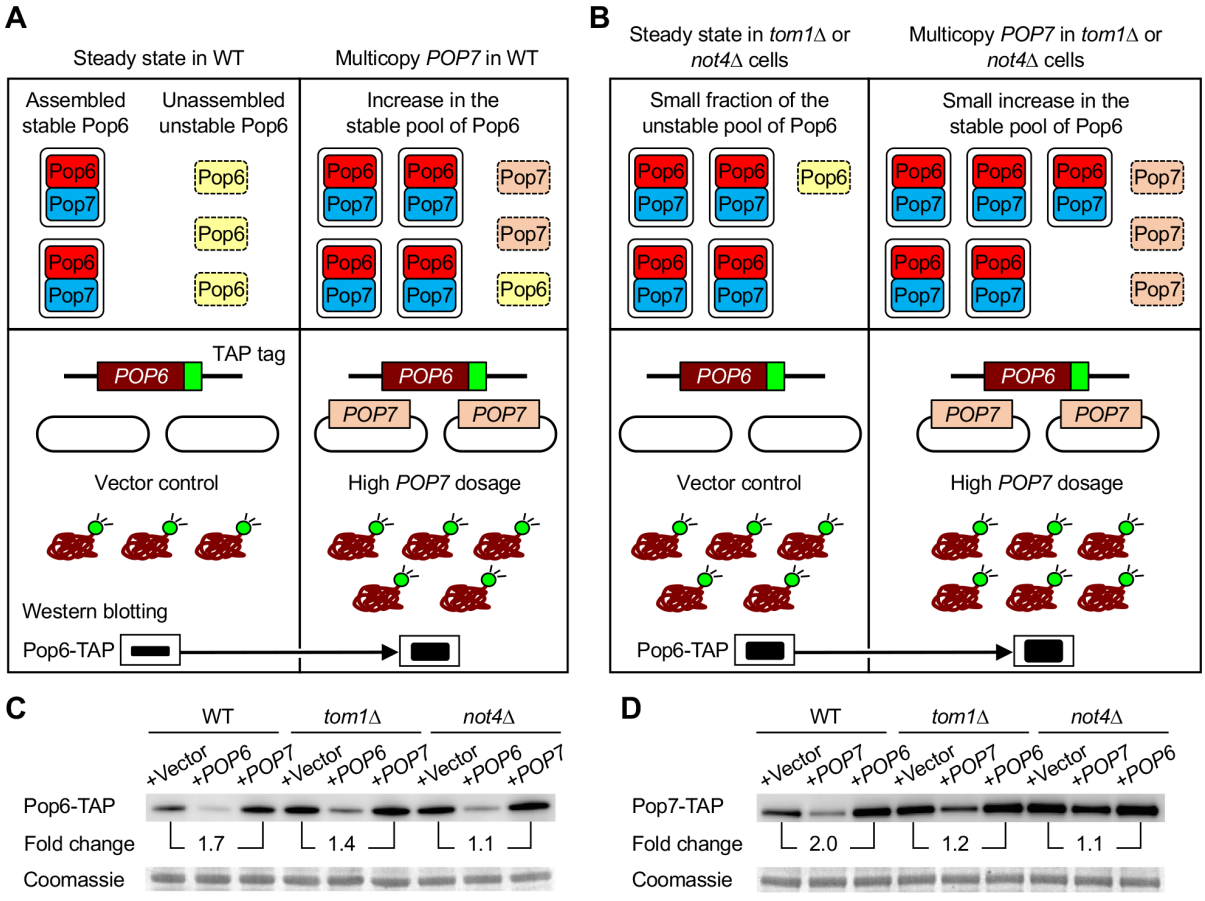

216
217
218 **Fig 3. Bidirectional dosage compensation of the Pop6–Pop7 heterodimeric subcomplex.**
219 (**A**) A model for stoichiometry control of Pop6 and Pop7 in WT cells (top) and an experi-
220 mental setup for testing this model (bottom). Pop6 becomes more stable when in complex
221 with the partner subunit Pop7, while unassembled Pop6 is less stable (top left). Upon multi-
222 copy expression of Pop7, potentially degraded Pop6 becomes stable by forming the complex
223 with excess Pop7 (top right). Pop6 level in vector control is the steady state level (bottom
224 left). If Pop6 turnover is reduced by high *POP7* dosage, Pop6 level is increased compared to
225 that in vector control (bottom right). (**B**) Same as in (**A**), except that shown is the case of
226 *tom1*Δ or *not4*Δ cells. Potentially degraded Pop6 in WT cells becomes stable in the absence
227 of Tom1 or Not4 responsible for Pop6 and Pop7 degradation, leading to an increase in the
228 Pop6–Pop7 complex (top left). Upon multicopy expression of Pop7, the remaining unstable
229 pool of Pop6 becomes stable by forming the complex with excess Pop7 (top right). The
230 steady state level of Pop6 in *tom1*Δ or *not4*Δ cells is higher than that in WT cells (bottom left).
231 If the turnover of Pop6 is further reduced by high *POP7* dosage, it leads to a small increase in
232 Pop6 level (bottom right). (**C, D**) Western blots of Pop6-TAP (**C**) and Pop7-TAP (**D**) in WT,
233 *tom1*Δ, and *not4*Δ cells. The TAP-tagged proteins were detected with PAP in the Single
234 (+Vector: pTOW40836) and Multi (+*POP6*: pTOW40836-*POP6*, +*POP7*:
235 pTOW40836-*POP7*) conditions. Quantification of band intensities relative to the Single con-
236 dition in each strain is shown. Coomassie staining of a 50-kDa protein, corresponding to
237 enolase, is shown as a loading control.

238 **NATs contribute to dosage compensation in a complex manner**
239 *S. cerevisiae* has five NATs: NatA, NatB, NatC, NatD, and NatE whose catalytic subunits are
240 respectively Naa10, Naa20, Naa30, Naa40, and Naa50 [29]. NATs have different sequence
241 specificities for N-acetylation and their substrates can be classified by the first two
242 N-terminal residues except NatD that recognizes approximately five-residue sequence motifs
243 [18, 29, 30]. As shown in Fig 4A, based on a prediction from N-terminal amino acids, the
244 RNase P/MRP subunits can be N-acetylated by NatA, NatB, or NatC. We examined whether
245 the RNase P/MRP subunits are less compensated in *naa10*Δ, *naa20*Δ, *naa30*Δ, *naa40*Δ, or
246 *naa50*Δ cells using the same experimental setup described in Fig 1B. Our experiments
247 showed that Pop4 and Rmp1 in *naa10*Δ (Fig 4B and 4C) and Pop6, Pop8, Rpr2, and Rmp1 in
248 *naa20*Δ (Fig 4D and 4E) were significantly less compensated than those in WT cells, while
249 all tested subunits were compensated in *naa30*Δ or *naa50*Δ as well as in WT cells (Fig 4F, 4G,
250 4J, and 4K). Only Pop3 was uncompensated in *naa40*Δ cells (Fig 4H and 4I), and the half-life
251 of Pop3 was prolonged upon increasing *POP3* copy number in *naa40*Δ cells (S4A and S4B
252 Fig). Of note, Pop3 was stabilized in *naa10*Δ compared to WT cells with or without an in-
253 crease in gene copy number (S5 Fig) ($p<0.05$, two-tailed Welch's *t* test), suggesting the in-
254 volvement of NatA in Pop3 degradation even in unperturbed conditions. We also found that
255 Pop5 compensation was more pronounced in *naa10*Δ than in WT cells (Fig 4B and 4C), sug-
256 gesting that accelerated Pop5 degradation during dosage compensation is blocked by NatA.
257
258 We summarized the contribution of each NAT, leading to several findings (Fig 4L; Table 1).
259 First, NatB-mediated compensation of Rmp1 is the only case that can be expected from its
260 N-terminal sequence. Second, conversely, the compensation of Pop4 and Pop6 were engaged
261 with NatA and NatB but not NatB and NatC, respectively. Additionally, Pop8 and Rpr2 were
262 subjected to the compensation mediated by NatB but not NatA. Third, Rmp1 was compen-
263 sated through multiple NATs, NatA and NatB. Fourth, the compensation of Pop3 was due in
264 large part to NatD but not NatA. Fifth, NATs were not identified for the compensation of
265 Pop7 and Rpp1. Finally, NATs-mediated compensation of the RNase P/MRP subunits was
266 mainly mediated by NatA and NatB, although their impact on protein levels was limited.
267 Taken together, the N-terminal sequence cannot simply explain NATs-mediated dosage com-
268 pensation. In all cases except for Pop3 and Pop8, the sum of the contribution of each NAT did
269 not reach to uncompensated protein level, suggesting that the stoichiometry control system
270 depends only partially on NATs-mediated dosage compensation.

271 **Table 1. Responsible E3 ubiquitin ligases and NATs for dosage compensation of the**
272 **RNase P/MRP subunits.**

Subunit	N-terminal first five amino acids	Responsible E3 Tom1 or Not4	Responsible NATs Sequence-based	Responsible NATs Experiment-based
Pop1	MSGSL	n.d.	NatA	n.d.
Pop3	MSGSL	not identified	NatA	NatD
Pop4	MDRTQ	Tom1, Not4	NatB	NatA
Pop5	MVRLK	Tom1, Not4	NatA	NatA[b]
Pop6	MINGV	Tom1	NatC	NatB
Pop7	MALKK	Tom1, Not4	NatA	not identified
Pop8	MGKKT	Tom1	NatA	NatB
Rpp1	MLVDL	Tom1, Not4	NatC	not identified
Rpr2	MGKKA	Tom1[a]	NatA	NatB
Snm1	MNKDQ	n.d.	NatB	n.d.
Rmp1	MDEMD	Tom1[a], Not4	NatB	NatA, NatB

273 [a] Marginally significant (p<0.1, two-tailed Welch's t test)
274 [b] Pop5 was significantly more compensated in *naa10*Δ than in WT cells.
275 n.d.: not detected

276 **Figure 4**

277

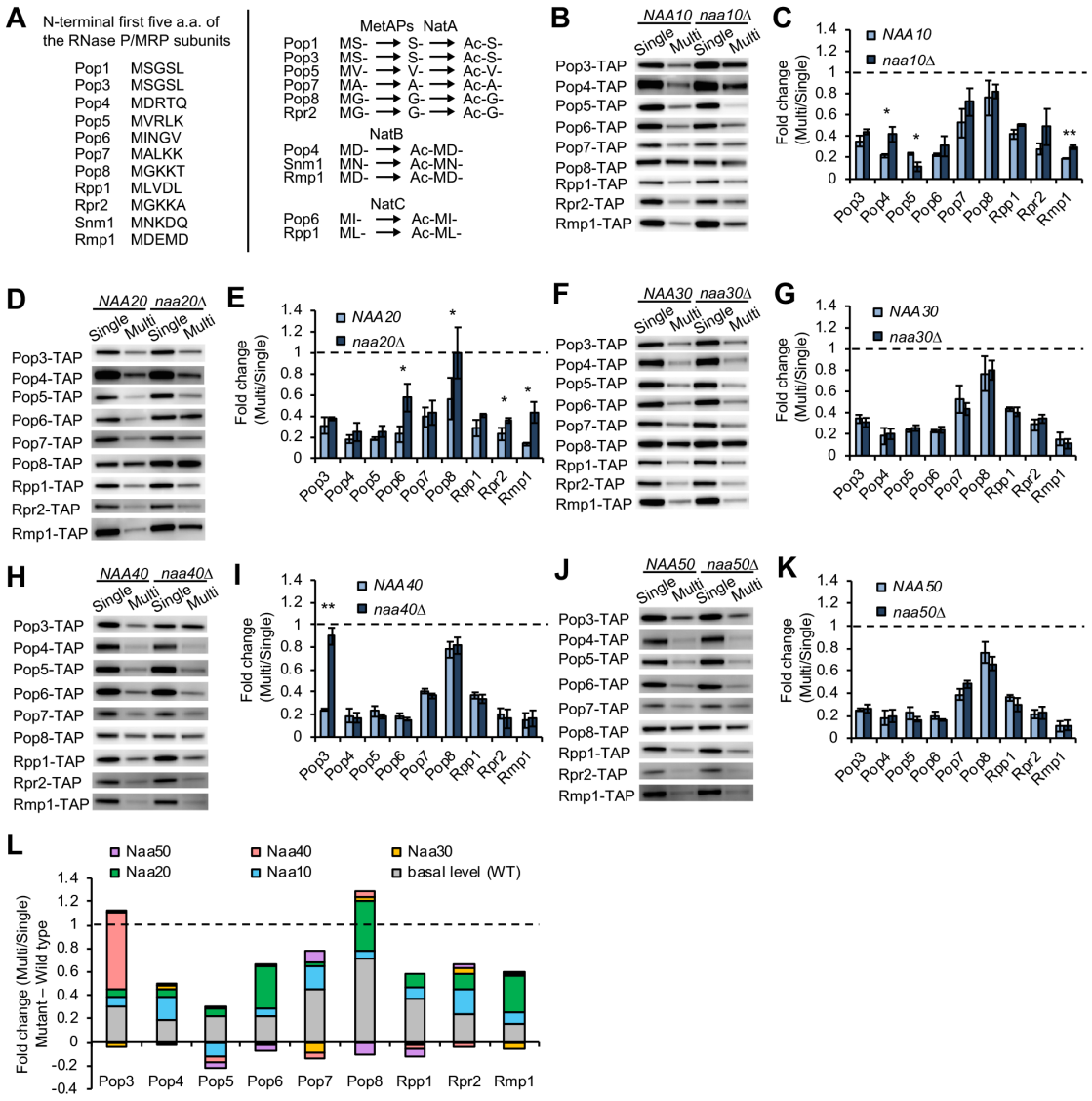

278

279

280 **Fig 4. NATs contribute to dosage compensation in a complex manner.**

281 (**A**) The first five amino acids of the RNase P/MRP subunits (left). Based on these sequences,
282 NatA, NatB, or NatC are responsible for their N-acetylation (right). NatA-mediated acetyla-
283 tion requires removal of N-terminal Methionine by Met-aminopeptidases Map1 and Map2
284 (MetAPs). (**B**) Western blots of the RNase P/MRP subunits in *naa10*Δ cells. The TAP-tagged
285 subunit expressed from the chromosome was detected with PAP. Pop1 and Snm1 were not
286 detected in our experiments. A representative blot from three biological replicates is shown.
287 (**C**) Quantification of protein levels in the Multi condition relative to those in the Single con-
288 dition in WT and *naa10*Δ cells. The average fold change ± s.d. was calculated from three bi-
289 ological replicates. Statistical significance was determined by a two-tailed Welch's *t* test
290 ($^{*}p<0.05$, $^{**}p<0.01$). Dashed line represents the same expression level between the Single and
291 Multi conditions. (**D–K**) Same as in (**B, C**), except that shown are Western blots of the RNase
292 P/MRP subunits and their quantification in *naa20*Δ (**D, E**), *naa30*Δ (**F, G**), *naa40*Δ (**H, I**), or
293 *naa50*Δ (**J, K**) cells. (**L**) Summary of the contribution of NATs to dosage compensation of the
294 RNase P/MRP subunits. The basal level is the average fold change in WT cells. The contribu-
295 tion of each NAT was calculated as the average fold change in each mutant minus the basal
296 level.

The first two N-terminal residues are not sufficient to determine the combination of NATs and E3 ligases in the Ac/N-end rule pathway

By summing the contribution of the tested E3 ligases and NATs to dosage compensation of the RNase P/MRP subunits, the protein level of all subunits except Pop5 reached to the uncompensated level (Fig 5A). Pop5 seems to be compensated through NATs-independent degradation pathway predominantly mediated by redundant control via Tom1 and No4 and/or unidentified E3 ligase(s). Pop4 and Pop7 were less compensated to the same degree in both *not4*Δ and *naa10*Δ cells (Fig 5). Because Not4 was previously identified as an N-recognin [11], these subunits may be compensated by the combination of NatA and Not4. Both Pop4 and Rmp1 are MD-starting proteins, but Rmp1 was compensated by not only NatA and Not4 but also NatB (Fig 2 and 4). Cog1 is also a MD-starting protein whose protein level is compensated by NatB and Not4 upon its overexpression [11]. These observations suggest that even though the first two N-terminal residues of substrate proteins are the same, the compensation through the Ac/N-end rule pathway occurs by different combinations of NATs and E3 ligases. Moreover, Rpp1 was almost fully uncompensated in *not4*Δ but not in all NATs mutants (Fig 2D and 2E), indicating that Not4-mediated compensation does not necessarily require NATs.

314 **Figure 5**
315

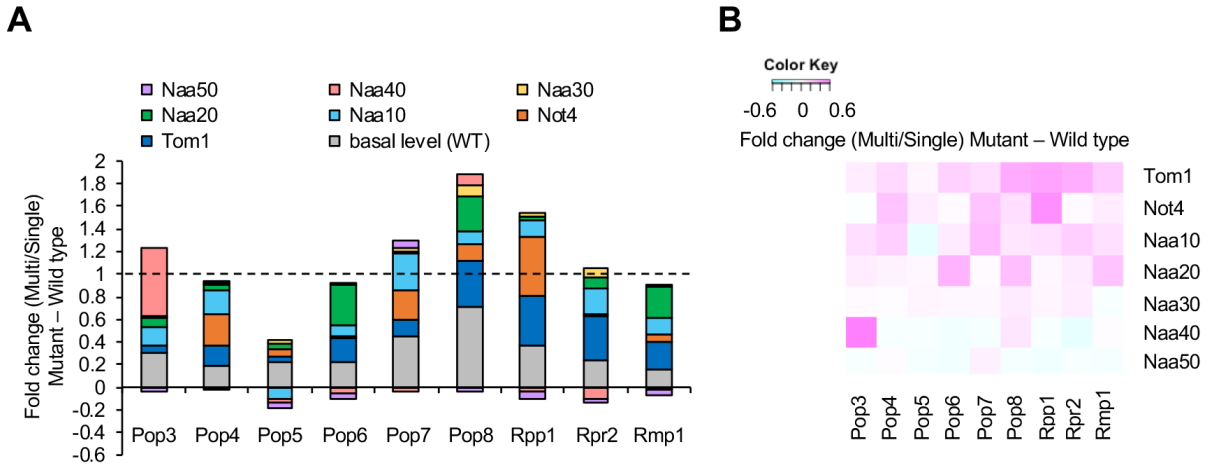

316
317
318 **Fig 5. Relative contribution of Tom1, Not4, and NATs to dosage compensation of the**
319 **RNase P/MRP subunits.**
320 (**A, B**) Summary of the contribution of Tom1, Not4, and NATs to dosage compensation of the
321 RNase P/MRP subunits. The basal level is the average fold change in WT cells. The contribu-
322 tion of each factor was calculated as the average fold change in each mutant minus the basal
323 level. Bar graph and the heat map show the same values.

Dosage compensation of histone H2A/H4 may not depend on the Ac/N-end rule pathway

As shown in Fig 4H and 4I, NatD efficiently contributes to the compensation of Pop3 that is not identified as a NatD substrate [31]. To further examine whether NATs-mediated dosage compensation is hardly predictable from N-terminal sequence, we next analyzed canonical NatD substrates. NatD is more selective than the other NATs [29], and only histone H2A/H4 subunits are identified as its substrates [31-33]. These histone subunits are MS-starting proteins that can be NatA substrates, but they are N-acetylated in the absence of Naa10 or its auxiliary subunit Naa15 [34]. Thus, we first tested whether NatD is involved in the compensation of histone H2A/H4 subunits: Hta2, Hhf1, and Hhf2. We found that they were subjected to dosage compensation even in the absence of Naa40 (Fig 6A–6C), suggesting that NatD is involved in their N-acetylation but not degradation. Additionally, the compensation was observed not only in *naa40*Δ but also in *naa10*Δ, *naa20*Δ, or *naa30*Δ as well as in WT cells (S6 Fig). We also found that they all were significantly less compensated in *tom1*Δ cells, although the degree of compensation was different among them (Fig 6A–6C). These results suggest that Tom1-mediated compensation of Hta2, Hhf1, and Hhf2 does not require NATs activity and that N-acetylation and dosage compensation are not necessarily linked. Therefore, dosage compensation of histone H2A/H4 may be mediated by N-acetylation-independent pathway.

NatD-mediated dosage compensation of a MH-starting protein Bet4

The selectivity of NatD-mediated N-acetylation comes from a sequence motif recognized by NatD and its substrate recognition site tailored for this motif [30]. The N-terminal of Pop3 is SGSL after removal of N-terminal Met by Met-aminopeptidases, which is different from the known motifs involved in histone subunits: SGGK (H2A) and SGRG (H4) [31]. We thus examined whether Bet2, which is a MSGSL-starting protein and a subunit of the Bet2–Bet4 heterodimer [35], is subjected to NatD-mediated compensation. We found that Bet2 was compensated by the same degree in either *naa40*Δ or WT cells (Fig 6D), indicating that the first MSGSL is not sufficient to trigger NatD-mediated compensation. Unexpectedly, Bet4 was remarkably less compensated in *naa40*Δ compared to WT cells (Fig 6E). Bet4 was indeed stable upon increasing *BET4* copy number in *naa40*Δ cells due to the prolonged half-life (S4C and S4D Fig). This phenomenon was surprising because Bet4 is a MH-starting protein that is virtually not N-acetylated while N-acetylation of Bet4 was detected but its responsible NATs were not identified [29, 36].

We further examined the contribution of the other NATs to Bet4 compensation and found that Bet4 was significantly less compensated in *naa20*Δ cells (Fig 6E). Thus, NatB and NatD are involved in Bet4 compensation. We also found an increase in Bet4 compensation in *naa10*Δ cells (Fig 6E), suggesting a NatA-mediated block of Bet4 degradation during the compensation. Although each of them is similar to Rmp1 in *naa10*Δ and *naa20*Δ and Pop5 in *naa10*Δ cells (Fig 4B–4E), both effects of NATs deletion were observed only for Bet4. Therefore, Bet4 was identified as the compensated protein whose stoichiometry is bidirectionally controlled by multiple NATs upon genetic perturbations.

365 **Figure 6**
366

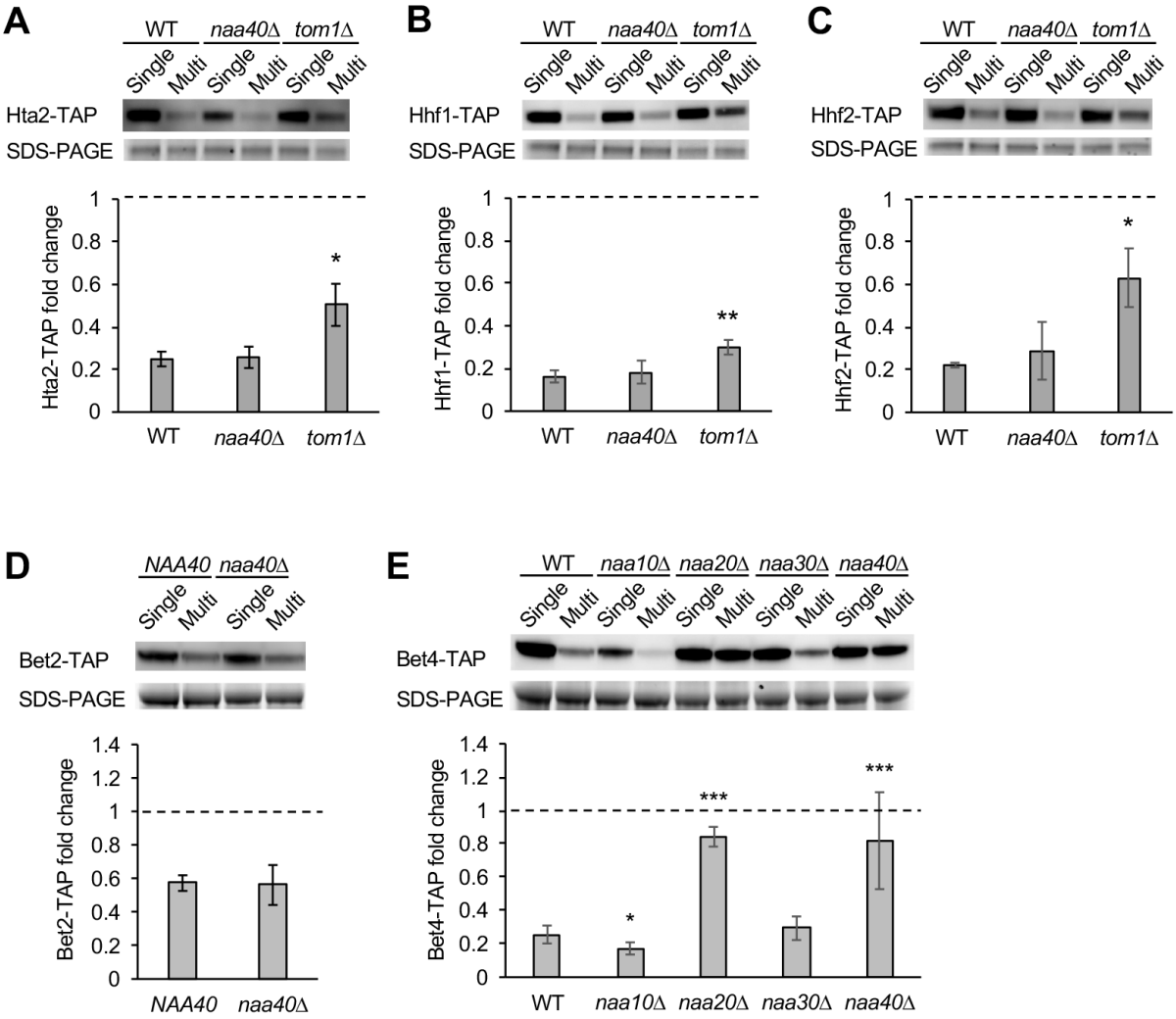

367
368
369 **Fig 6. Dissection of the complexity of NATs-mediated dosage compensation by focusing**
370 **on NatD.**
371 (**A–C**) Tom1-mediated dosage compensation of NatD substrates does not require Naa40.
372 Western blot analysis of histone H2A/H4: Hta2-TAP (**A**), Hhf1-TAP (**B**), and Hhf2-TAP (**C**)
373 in WT, *naa40*Δ, or *tom1*Δ cells. The TAP-tagged subunits were detected with PAP (top). The
374 average fold change ± s.d. was calculated from three biological replicates (bottom). Statistical
375 significance was determined by a two-tailed Welch's *t* test ($^{*}p<0.05$, $^{**}p<0.01$). Dashed line
376 represents the same expression level between the Single and Multi conditions. (**D**) Western
377 blot analysis of Bet2-TAP in *naa40*Δ cells. The TAP-tagged subunits were detected with PAP
378 (top). The average fold change ± s.d. was calculated from four biological replicates (bottom).
379 (**E**) Western blot analysis of Bet4-TAP in *naa10*Δ, *naa20*Δ, *naa30*Δ, and *naa40*Δ cells. The
380 TAP-tagged subunits were detected with PAP (top). The average fold change ± s.d. was cal-
381 culated from eight and three biological replicates for *naa40*Δ and the other mutants, respec-
382 tively (bottom) ($^{*}p<0.05$, $^{***}p<0.001$).

Discussion

To investigate how well the Ac/N-end rule pathway explains dosage compensation, we systematically measured the contribution of E3 ubiquitin ligases and NATs to the compensation of the RNase P/MRP subunits (Fig 2 and 4). Our data consisting of 18 subunits and 10 quality control factors, in total 100 combinations, demonstrated that multiple E3 ubiquitin ligases and NATs are involved in the compensation. NATs-mediated compensation was observed for 7 out of 14 subunits of the RNase P/MRP, histone, and Bet2–Bet4 complexes (Fig 4 and 6). However, given that the lack of NATs did not completely reduce the compensation of the tested subunits except for Pop3 in *naa40*Δ and Bet4 in *naa20*Δ and *naa40*Δ cells, stoichiometry control of multiprotein complexes depends only partially on the Ac/N-end rule pathway.

In this study, we manipulated gene copy number to perturb cellular systems and elucidate mechanisms for buffering gene expression perturbations. Our data showed that NATs contribute to proteolysis upon exogenous overexpression of the RNase P/MRP subunits, whereas without overexpression the endogenous protein levels were almost not affected in NATs mutants compared to E3 mutants (Fig 2C and 2F and S5 Fig). This is consistent with a recent comprehensive analysis showing that N-acetylation rarely acts as a degradation signal in physiological conditions in yeast [37]. In agreement with these findings, a limited number of subunits are physiologically synthesized in excess compared to stoichiometry and the half-life of such subunits tends to be faster than that of proportionally synthesized subunits [13, 14]. Therefore, NATs-mediated dosage compensation may be a fail-safe mechanism that is rarely and predominantly triggered by genetic perturbations or physiological overexpression causing stoichiometric imbalance.

We identified Tom1 as a factor of the stoichiometry control system (Fig 2A and 2B), which is consistent with Tom1-mediated degradation of excess ribosomal subunits [19]. It should be noted that, as discussed in [19], basic isoelectric point is a common characteristic of known Tom1 substrates (Cdc6, Hht2, Yra1, and Rpl26a) and the RNase P/MRP subunits except Pop8 (S7 Fig) [19, 38-40]. The weak electrical interaction between Tom1 with acidic isoelectric point and Pop8 might explain why the compensation degree of Pop8 is lower than the other subunits. Additionally, these substrates as well as Tom1 are nucleic acid binding and localize in the nucleus [41]. These characteristics suggest that Tom1 is broadly responsible for the compensation of nucleic acid binding subunits.

We found that ribosome-associated factors Not4 and NATs were involved in dosage compensation of the RNase P/MRP subunits (Fig 2D, 2E, and 4), which is consistent with the stabilization of Cog1 in *not4*Δ or *naa20*Δ cells upon its overexpression [11, 42-44]. These observations and cotranslational ubiquitination of a subset of the proteome suggest the possibility of cotranslational dosage compensation [45, 46]. This is also supported by the findings that multiprotein complex subunits tend to assemble cotranslationally and that such subunits are prone to aggregation and degradation in the absence of their partner subunits [47, 48]. Therefore, future investigations of this possibility may gain insight into the hierarchy of the multi-layered stoichiometry control system.

We described the complexity of the stoichiometry control system (Fig 5 and 6, Table 1), as (i) multiple E3 ligases Tom1 and Not4 are involved in the compensation of Pop4, Pop5, Pop7, Rpp1, and Rmp1, (ii) N-terminal sequence is not necessarily a determinant of which NATs contribute to dosage compensation, and (iii) multiple NATs are involved in the compensation of Rmp1 and Bet4. Robust control of Rmp1 seems to be due to its C-terminal polylysine se-

quence CKKKKKRKKKNK that induces translation arrest coupled with Not4-mediated proteolysis [49]. Our findings thus suggest that the complexity of this system reflects its robustness. Furthermore, as argued in [50], other mechanisms for sensing unassembled subunits and correcting stoichiometric imbalance may exist. For example, the most recent study showed that protein aggregation of excess subunits functions as the compensation pathway in aneuploid yeast cells [51]. It is also possible to speculate that substrate recognition by one NAT is partially redundant with the other NAT because of the remarkable reduction of Bet4 compensation in both NatB and NatD mutants and functional redundancy between yeast NatC and human NatF (Fig 6E) [52].

The compensation of Pop3 in *naa40*Δ and Bet4 in *naa20*Δ and *naa40*Δ cells was almost fully reduced (Fig 4H, 4I, and 6E), supporting the dependency of stoichiometry control on the Ac/N-end rule pathway [11]. However, these are rare cases in our study and the first examples of NatD-mediated dosage compensation. Indeed, canonical NatD substrates histone H2A/H4 were compensated even in the absence of Naa40 (Fig 6A–6C). Importantly, consistent with the stabilization of histone H3 subunit Hht2 by *TOM1* deletion [39], H2A/H4 were less compensated in *tom1*Δ cells. These results suggest that unassembled subunits are selectively degraded by not only the Ac/N-end rule but also other pathways. This is further suggested by the observation that Rpp1 compensation involves Tom1 and Not4 but not NATs (Fig 5, Table 1).

We also found that Pop5 and Bet4 were destabilized when they were overexpressed in *naa10*Δ cells (Fig 4B, 4C, and 6E). Similarly, previous studies showed that proteins with unacetylated N-terminal Met followed by a small hydrophobic residue and MN-starting proteins are destabilized in *naa30*Δ and *naa20*Δ cells, respectively, by the Arg/N-end rule pathway [37, 53]. However, because N-terminal sequence of Pop5 (MV) and Bet4 (MH) are not appropriate for these cases, their degradation in *naa10*Δ cells might be accelerated by unknown mechanisms. We speculate that complex stoichiometry is robustly maintained by switching degradation pathways in response to perturbations in the stoichiometry control system. Indeed, the interplay between the Arg/N-end rule and the Ac/N-end rule pathways was proposed based on the observation that the short-lived reporter protein and Msn4 are synergistically stabilized in double mutants *naa20*Δ *ubr1*Δ and *naa30*Δ *ubr1*Δ, respectively [53, 54].

Quality control of multiprotein complexes impacts a broad range of biological processes because of the fact that cellular systems are based on functional complexes. For example, the RNase P and MRP complexes are responsible for maturation of tRNA and rRNA, respectively [26]. Additionally, Pop1, Pop6, and Pop7 are shared with telomerase [55]. Our finding of robust control of dosage balance between Pop6 and Pop7 seems to be in line with their functional importance (Fig 3). More generally, dosage compensation may play a role as a fail-safe mechanism for shaping proteome stoichiometry as discussed above. In agreement with this concept, paralogous complex subunits tend to be compensated each other for modulating protein interactome [56, 57]. Furthermore, proteolysis-mediated compensation perversely corrects physiologically caused stoichiometric imbalance during meiosis [58], which may explain how cells cope with a subset of subunits overexpressed in unperturbed conditions [13]. Therefore, further dissection of the complexity and working principles of the stoichiometry control system will help to describe cellular robustness.

Materials and Methods

Strains, plasmids, and media

For construction of mutant strains lacking a gene encoding the E3 ubiquitin ligase (*TOM1* or *NOT4*) or N-aetyltransferase (*NAA10*, *NAA20*, *NAA30*, *NAA40*, or *NAA50*) and carrying a TAP-tagged gene of interest, the deletion collection and the TAP collection of haploid yeast (Dharmacon) were used. BY4741 carrying Pop4-TAP, Rmp1-TAP, or Bet4-TAP were constructed in this study. Genomic DNA of each single deletion strain was extracted, and then, each locus replaced with the *kanMX4* cassette was amplified by PCR with a primer library prepared in our previous study [5]. The TAP-tagged strains were transformed with the PCR products by the lithium acetate method and selected on YPD plates containing G418 (200 μg/mL). For construction of plasmids, DNA fragment of each target region was amplified from the genome and cloned into pTOW40836 by homologous recombination in BY4741 cells. The TAP-tagged strains described above were transformed with the plasmids and selected on SC medium lacking uracil.

Measurement of plasmid copy number

The plasmid copy number was measured by the gTOW technique [59]. The cells grown at log-phase for Western blotting were harvested for the gTOW analysis from the same culture. In short, 200 μL of the culture was centrifuged and the pelleted cells were suspended in 100 μL of zymolyase solution [2.5 mg/mL Zymolyase-100T dissolved in 1.2 M sorbitol, 10 mM sodium phosphate (pH7.5)] and incubated at 37 °C for 15 min for DNA extraction. The suspension was heated at 100 °C for 10 min, cooled at –80 °C for 10 min, and again heated at 100 °C for 10 min. After cooling down to RT followed by a centrifugation, the supernatant was subjected to real-time quantitative PCR with Lightcycler 480 (Roche). The primers for *LEU3* on the genome or *leu2d* gene on pTOW40836 and SYBR Green I Master (Roche) were used for the PCR. The resulting plasmid copy number was calculated based on the expression levels of *LEU3* and *leu2d* genes according to the method described previously [59].

Western blot analysis

Cells were grown at 30 °C in 2 mL of SC–Ura medium for overnight and then measured the optical density at 600 nm (OD_{600}) and inoculated into fresh medium at initial OD_{600} of 0.5 in 3 mL. After 4 h, 1 OD_{600} units were harvested at log-phase when OD_{600} was around 1. The cells were treated with 1 mL of 0.2 N NaOH for 5 min at room temperature (RT) and centrifuged at 15,000 rpm for 1 min. The pelleted cells were suspended in 50 μL of 1× NuPAGE LDS Sample Buffer (Invitrogen) containing 100 mM DTT and heated at 100 °C for 5 min. For the analysis of the TAP-tagged proteins, two-fold serially diluted lysates were analyzed as described below, and we confirmed that 0.025 OD_{600} units provide appropriate signal in the linear range. The extract diluted 8-fold with 1× NuPAGE LDS Sample Buffer, corresponding with 0.025 OD_{600} units, was separated by polyacrylamide gel electrophoresis with lithium dodecyl sulfate (SDS-PAGE) on NuPAGE 4%–12% Bis-Tris Gel (Invitrogen). For the analysis of the GFP-tagged proteins, 0.2 OD_{600} units were subjected to SDS-PAGE. The separated proteins were transferred onto PVDF membrane using the iBlot Transfer Stack PVDF membrane (Invitrogen). The blotted membrane was treated with PBST [1× PBS, 0.1% Tween 20] for 10 min, and then blocked with 4% skim milk in PBST for 1 h at RT. The TAP-tagged proteins were probed with PAP (Sigma-Aldrich) (1:2,000) for 1 h at RT. The GFP-tagged proteins were probed with anti-GFP antibody (Roche) (1:1,000) and peroxidase-conjugated secondary antibody (Nichirei Biosciences) (1:1,000) for 1 h at RT. After washing the membrane with PBST for 5 min for three times, chemiluminescence was induced by adding 500 μL of SuperSignal West Femto Maximum Sensitivity Substrate (Ther-

530 mo Scientific) on the membrane and detected using LAS-4000 image analyzer (Fujifilm) and
531 ImageQuant LAS 4000 (GE Healthcare). Quantification of the band intensity was carried out
532 using ImageQuant TL (GE Healthcare) and the fold change was calculated after background
533 subtraction. After washing the membrane with sterile water for 5 min for three times, total
534 proteins were visualized by Coomassie staining with SimplyBlue SafeStain (Invitrogen) to
535 confirm equal loading of proteins. The stained membrane was digitized using LAS-4000 im-
536 age analyzer and ImageQuant LAS 4000.
537
538 For the analysis of histone H2A/H4 and the Bet2–Bet4 heterodimer, the harvested cells were
539 treated with 1 mL of 0.2 N NaOH for 5 min at RT. Cells were suspended in 1× NuPAGE LDS
540 Sample Buffer (Invitrogen) and then heated at 70 °C for 10 min. The supernatant corre-
541 sponding to 0.5 OD_{600} units was labeled with EzLabel FluoroNeo (ATTO) and subjected to
542 SDS-PAGE, followed by Western blot with PAP (Sigma-Aldrich) (1:2,000) as described
543 above.
544
545 **Cycloheximide chase assay**
546 The degradation rate of Pop3 and Bet4 was measured as previously described [7]. Briefly, the
547 log-phase culture corresponding to 1 OD_{600} unit of cells was harvested for time point 0 and
548 afterwards CHX was added to a final concentration of 200 µg/mL. Cells were harvested after
549 1, 2, 4, and 6.5 h, followed by total protein extraction in 1× NuPAGE LDS Sample Buffer.
550 The supernatant corresponding to 0.5 OD_{600} units was subjected to Western blot analysis us-
551 ing PAP as described above. The remaining protein level at each time point was calculated
552 against that at time point 0.

Acknowledgments

We thank the members of Moriya laboratory for their support.

556 **References**
557

558 1. Zheng XY, O'Shea EK. Cyanobacteria Maintain Constant Protein Concentration
559 despite Genome Copy-Number Variation. Cell Rep. 2017;19(3):497-504. Epub
560 2017/04/20. doi: 10.1016/j.celrep.2017.03.067. PubMed PMID: 28423314.
561 2. Kafri M, Metzl-Raz E, Jona G, Barkai N. The Cost of Protein Production. Cell Rep.
562 2016;14(1):22-31. Epub 2016/01/05. doi: 10.1016/j.celrep.2015.12.015. PubMed
563 PMID: 26725116; PubMed Central PMCID: PMCPMC4709330.
564 3. Dill KA, Ghosh K, Schmit JD. Physical limits of cells and proteomes. Proc Natl Acad
565 Sci U S A. 2011;108(44):17876-82. Epub 2011/10/19. doi: 10.1073/pnas.1114477108.
566 PubMed PMID: 22006304; PubMed Central PMCID: PMCPMC3207669.
567 4. Sopko R, Huang D, Preston N, Chua G, Papp B, Kafadar K, et al. Mapping pathways
568 and phenotypes by systematic gene overexpression. Mol Cell. 2006;21(3):319-30.
569 Epub 2006/02/04. doi: 10.1016/j.molcel.2005.12.011. PubMed PMID: 16455487.
570 5. Makanae K, Kintaka R, Makino T, Kitano H, Moriya H. Identification of
571 dosage-sensitive genes in Saccharomyces cerevisiae using the genetic tug-of-war
572 method. Genome Res. 2013;23(2):300-11. Epub 2013/01/01. doi:
573 10.1101/gr.146662.112. PubMed PMID: 23275495; PubMed Central PMCID:
574 PMCPMC3561871.
575 6. Moriya H. Quantitative nature of overexpression experiments. Mol Biol Cell.
576 2015;26(22):3932-9. Epub 2015/11/07. doi: 10.1091/mbc.E15-07-0512. PubMed
577 PMID: 26543202; PubMed Central PMCID: PMCPMC4710226.
578 7. Ishikawa K, Makanae K, Iwasaki S, Ingolia NT, Moriya H. Post-Translational Dosage
579 Compensation Buffers Genetic Perturbations to Stoichiometry of Protein Complexes.
580 PLoS Genet. 2017;13(1):e1006554. Epub 2017/01/26. doi:
581 10.1371/journal.pgen.1006554. PubMed PMID: 28121980; PubMed Central PMCID:
582 PMCPMC5266272.
583 8. Stingele S, Stoehr G, Peplowska K, Cox J, Mann M, Storchova Z. Global analysis of
584 genome, transcriptome and proteome reveals the response to aneuploidy in human
585 cells. Mol Syst Biol. 2012;8:608. Epub 2012/09/13. doi: 10.1038/msb.2012.40.
586 PubMed PMID: 22968442; PubMed Central PMCID: PMCPMC3472693.
587 9. Dephoure N, Hwang S, O'Sullivan C, Dodgson SE, Gygi SP, Amon A, et al.
588 Quantitative proteomic analysis reveals posttranslational responses to aneuploidy in
589 yeast. Elife. 2014;3:e03023. Epub 2014/07/31. doi: 10.7554/eLife.03023. PubMed
590 PMID: 25073701; PubMed Central PMCID: PMCPMC4129440.
591 10. Torres EM, Sokolsky T, Tucker CM, Chan LY, Boselli M, Dunham MJ, et al. Effects
592 of aneuploidy on cellular physiology and cell division in haploid yeast. Science.
593 2007;317(5840):916-24. Epub 2007/08/19. doi: 10.1126/science.1142210. PubMed
594 PMID: 17702937.
595 11. Shemorry A, Hwang CS, Varshavsky A. Control of protein quality and stoichiometries
596 by N-terminal acetylation and the N-end rule pathway. Mol Cell. 2013;50(4):540-51.
597 Epub 2013/04/23. doi: 10.1016/j.molcel.2013.03.018. PubMed PMID: 23603116;
598 PubMed Central PMCID: PMCPMC3665649.
599 12. Papp B, Pal C, Hurst LD. Dosage sensitivity and the evolution of gene families in
600 yeast. Nature. 2003;424(6945):194-7. Epub 2003/07/11. doi: 10.1038/nature01771.
601 PubMed PMID: 12853957.
602 13. Li GW, Burkhardt D, Gross C, Weissman JS. Quantifying absolute protein synthesis
603 rates reveals principles underlying allocation of cellular resources. Cell.
604 2014;157(3):624-35. Epub 2014/04/29. doi: 10.1016/j.cell.2014.02.033. PubMed
605 PMID: 24766808; PubMed Central PMCID: PMCPMC4006352.

606 14. Taggart JC, Li GW. Production of Protein-Complex Components Is Stoichiometric
607 and Lacks General Feedback Regulation in Eukaryotes. Cell Syst. 2018. Epub
608 2018/12/17. doi: 10.1016/j.cels.2018.11.003. PubMed PMID: 30553725.
609 15. Ingolia NT, Hussmann JA, Weissman JS. Ribosome Profiling: Global Views of
610 Translation. Cold Spring Harb Perspect Biol. 2018. Epub 2018/07/25. doi:
611 10.1101/cshperspect.a032698. PubMed PMID: 30037969.
612 16. Sung MK, Reitsma JM, Sweredoski MJ, Hess S, Deshaies RJ. Ribosomal proteins
613 produced in excess are degraded by the ubiquitin-proteasome system. Mol Biol Cell.
614 2016;27(17):2642-52. Epub 2016/07/08. doi: 10.1091/mbc.E16-05-0290. PubMed
615 PMID: 27385339; PubMed Central PMCID: PMCPMC5007085.
616 17. Yanagitani K, Juszkiewicz S, Hegde RS. UBE2O is a quality control factor for
617 orphans of multiprotein complexes. Science. 2017;357(6350):472-5. Epub 2017/08/05.
618 doi: 10.1126/science.aan0178. PubMed PMID: 28774922; PubMed Central PMCID:
619 PMCPMC5549844.
620 18. Hwang CS, Shemorry A, Varshavsky A. N-terminal acetylation of cellular proteins
621 creates specific degradation signals. Science. 2010;327(5968):973-7. Epub
622 2010/01/30. doi: 10.1126/science.1183147. PubMed PMID: 20110468; PubMed
623 Central PMCID: PMCPMC4259118.
624 19. Sung MK, Porras-Yakushi TR, Reitsma JM, Huber FM, Sweredoski MJ, Hoelz A, et
625 al. A conserved quality-control pathway that mediates degradation of unassembled
626 ribosomal proteins. Elife. 2016;5. Epub 2016/08/24. doi: 10.7554/eLife.19105.
627 PubMed PMID: 27552055; PubMed Central PMCID: PMCPMC5026473.
628 20. Aksnes H, Ree R, Arnesen T. Co-translational, Post-translational, and Non-catalytic
629 Roles of N-Terminal Acetyltransferases. Mol Cell. 2019;73(6):1097-114. Epub
630 2019/03/18. doi: 10.1016/j.molcel.2019.02.007. PubMed PMID: 30878283.
631 21. Nguyen KT, Lee CS, Mun SH, Truong NT, Park SK, Hwang CS. N-terminal
632 acetylation and the N-end rule pathway control degradation of the lipid droplet
633 protein PLIN2. J Biol Chem. 2019;294(1):379-88. Epub 2018/11/15. doi:
634 10.1074/jbc.RA118.005556. PubMed PMID: 30425097; PubMed Central PMCID:
635 PMCPMC6322874.
636 22. Varshavsky A. The N-end rule pathway and regulation by proteolysis. Protein Sci.
637 2011;20(8):1298-345. Epub 2011/06/03. doi: 10.1002/pro.666. PubMed PMID:
638 21633985; PubMed Central PMCID: PMCPMC3189519.
639 23. Harper JW, Bennett EJ. Proteome complexity and the forces that drive proteome
640 imbalance. Nature. 2016;537(7620):328-38. Epub 2016/09/16. doi:
641 10.1038/nature19947. PubMed PMID: 27629639; PubMed Central PMCID:
642 PMCPMC5204264.
643 24. Gardner RG, Nelson ZW, Gottschling DE. Degradation-mediated protein quality
644 control in the nucleus. Cell. 2005;120(6):803-15. Epub 2005/03/31. doi:
645 10.1016/j.cell.2005.01.016. PubMed PMID: 15797381.
646 25. Bartel B, Wunning I, Varshavsky A. The recognition component of the N-end rule
647 pathway. EMBO J. 1990;9(10):3179-89. Epub 1990/10/01. PubMed PMID: 2209542;
648 PubMed Central PMCID: PMCPMC552047.
649 26. Esakova O, Krasilnikov AS. Of proteins and RNA: the RNase P/MRP family. RNA.
650 2010;16(9):1725-47. Epub 2010/07/16. doi: 10.1261/rna.2214510. PubMed PMID:
651 20627997; PubMed Central PMCID: PMCPMC2924533.
652 27. Perederina A, Esakova O, Koc H, Schmitt ME, Krasilnikov AS. Specific binding of a
653 Pop6/Pop7 heterodimer to the P3 stem of the yeast RNase MRP and RNase P RNAs.
654 RNA. 2007;13(10):1648-55. Epub 2007/08/25. doi: 10.1261/rna.654407. PubMed
655 PMID: 17717080; PubMed Central PMCID: PMCPMC1986809.

656 28. Perederina A, Esakova O, Quan C, Khanova E, Krasilnikov AS. Eukaryotic
657 ribonucleases P/MRP: the crystal structure of the P3 domain. EMBO J.
658 2010;29(4):761-9. Epub 2010/01/16. doi: 10.1038/emboj.2009.396. PubMed PMID:
659 20075859; PubMed Central PMCID: PMCPMC2829168.
660 29. Aksnes H, Drazic A, Marie M, Arnesen T. First Things First: Vital Protein Marks by
661 N-Terminal Acetyltransferases. Trends Biochem Sci. 2016;41(9):746-60. Epub
662 2016/08/09. doi: 10.1016/j.tibs.2016.07.005. PubMed PMID: 27498224.
663 30. Magin RS, Liszczak GP, Marmorstein R. The molecular basis for histone H4- and
664 H2A-specific amino-terminal acetylation by NatD. Structure. 2015;23(2):332-41.
665 Epub 2015/01/27. doi: 10.1016/j.str.2014.10.025. PubMed PMID: 25619998; PubMed
666 Central PMCID: PMCPMC4318724.
667 31. Song OK, Wang X, Waterborg JH, Sternglanz R. An Nalpha-acetyltransferase
668 responsible for acetylation of the N-terminal residues of histones H4 and H2A. J Biol
669 Chem. 2003;278(40):38109-12. Epub 2003/08/14. doi: 10.1074/jbc.C300355200.
670 PubMed PMID: 12915400.
671 32. Hole K, Van Damme P, Dalva M, Aksnes H, Glomnes N, Varhaug JE, et al. The
672 human N-alpha-acetyltransferase 40 (hNaa40p/hNatD) is conserved from yeast and
673 N-terminally acetylates histones H2A and H4. PLoS One. 2011;6(9):e24713. Epub
674 2011/09/22. doi: 10.1371/journal.pone.0024713. PubMed PMID: 21935442; PubMed
675 Central PMCID: PMCPMC3174195.
676 33. Polevoda B, Hoskins J, Sherman F. Properties of Nat4, an N(alpha)-acetyltransferase
677 of Saccharomyces cerevisiae that modifies N termini of histones H2A and H4. Mol
678 Cell Biol. 2009;29(11):2913-24. Epub 2009/04/01. doi: 10.1128/MCB.00147-08.
679 PubMed PMID: 19332560; PubMed Central PMCID: PMCPMC2682015.
680 34. Mullen JR, Kayne PS, Moerschell RP, Tsunasawa S, Gribskov M, Colavito-Shepanski
681 M, et al. Identification and characterization of genes and mutants for an N-terminal
682 acetyltransferase from yeast. EMBO J. 1989;8(7):2067-75. Epub 1989/07/01.
683 PubMed PMID: 2551674; PubMed Central PMCID: PMCPMC401092.
684 35. Jiang Y, Rossi G, Ferro-Novick S. Bet2p and Mad2p are components of a
685 prenyltransferase that adds geranylgeranyl onto Ypt1p and Sec4p. Nature.
686 1993;366(6450):84-6. Epub 1993/11/04. doi: 10.1038/366084a0. PubMed PMID:
687 8232542.
688 36. Van Damme P, Lasa M, Polevoda B, Gazquez C, Elosegui-Artola A, Kim DS, et al.
689 N-terminal acetylome analyses and functional insights of the N-terminal
690 acetyltransferase NatB. Proc Natl Acad Sci U S A. 2012;109(31):12449-54. Epub
691 2012/07/21. doi: 10.1073/pnas.1210303109. PubMed PMID: 22814378; PubMed
692 Central PMCID: PMCPMC3412031.
693 37. Kats I, Khmelinskii A, Kschonsak M, Huber F, Kniess RA, Bartosik A, et al. Mapping
694 Degradation Signals and Pathways in a Eukaryotic N-terminome. Mol Cell.
695 2018;70(3):488-501 e5. Epub 2018/05/05. doi: 10.1016/j.molcel.2018.03.033.
696 PubMed PMID: 29727619.
697 38. Kim DH, Zhang W, Koepp DM. The Hect domain E3 ligase Tom1 and the F-box
698 protein Dia2 control Cdc6 degradation in G1 phase. J Biol Chem.
699 2012;287(53):44212-20. Epub 2012/11/07. doi: 10.1074/jbc.M112.401778. PubMed
700 PMID: 23129771; PubMed Central PMCID: PMCPMC3531737.
701 39. Singh RK, Kabbaj MH, Paik J, Gunjan A. Histone levels are regulated by
702 phosphorylation and ubiquitylation-dependent proteolysis. Nat Cell Biol.
703 2009;11(8):925-33. Epub 2009/07/07. doi: 10.1038/ncb1903. PubMed PMID:
704 19578373; PubMed Central PMCID: PMCPMC2720428.
705 40. Iglesias N, Tutucci E, Gwizdek C, Vinciguerra P, Von Dach E, Corbett AH, et al.

Ubiquitin-mediated mRNP dynamics and surveillance prior to budding yeast mRNA export. Genes Dev. 2010;24(17):1927-38. Epub 2010/09/03. doi: 10.1101/gad.583310. PubMed PMID: 20810649; PubMed Central PMCID: PMCPMC2932974.

41. Huh WK, Falvo JV, Gerke LC, Carroll AS, Howson RW, Weissman JS, et al. Global analysis of protein localization in budding yeast. Nature. 2003;425(6959):686-91. Epub 2003/10/17. doi: 10.1038/nature02026. PubMed PMID: 14562095.

42. Collart MA, Panasenko OO, Nikolaev SI. The Not3/5 subunit of the Ccr4-Not complex: a central regulator of gene expression that integrates signals between the cytoplasm and the nucleus in eukaryotic cells. Cell Signal. 2013;25(4):743-51. Epub 2013/01/03. doi: 10.1016/j.cellsig.2012.12.018. PubMed PMID: 23280189.

43. Starheim KK, Gevaert K, Arnesen T. Protein N-terminal acetyltransferases: when the start matters. Trends Biochem Sci. 2012;37(4):152-61. Epub 2012/03/13. doi: 10.1016/j.tibs.2012.02.003. PubMed PMID: 22405572.

44. Halter D, Collart MA, Panasenko OO. The Not4 E3 ligase and CCR4 deadenylase play distinct roles in protein quality control. PLoS One. 2014;9(1):e86218. Epub 2014/01/28. doi: 10.1371/journal.pone.0086218. PubMed PMID: 24465968; PubMed Central PMCID: PMCPMC3895043.

45. Wang F, Durfee LA, Huibregtse JM. A cotranslational ubiquitination pathway for quality control of misfolded proteins. Mol Cell. 2013;50(3):368-78. Epub 2013/04/16. doi: 10.1016/j.molcel.2013.03.009. PubMed PMID: 23583076; PubMed Central PMCID: PMCPMC3654026.

46. Duttler S, Pechmann S, Frydman J. Principles of cotranslational ubiquitination and quality control at the ribosome. Mol Cell. 2013;50(3):379-93. Epub 2013/04/16. doi: 10.1016/j.molcel.2013.03.010. PubMed PMID: 23583075; PubMed Central PMCID: PMCPMC3886275.

47. Shiber A, Doring K, Friedrich U, Klann K, Merker D, Zedan M, et al. Cotranslational assembly of protein complexes in eukaryotes revealed by ribosome profiling. Nature. 2018;561(7722):268-72. Epub 2018/08/31. doi: 10.1038/s41586-018-0462-y. PubMed PMID: 30158700.

48. Shieh YW, Minguez P, Bork P, Auburger JJ, Guilbride DL, Kramer G, et al. Operon structure and cotranslational subunit association direct protein assembly in bacteria. Science. 2015;350(6261):678-80. Epub 2015/09/26. doi: 10.1126/science.aac8171. PubMed PMID: 26405228.

49. Dimitrova LN, Kuroha K, Tatematsu T, Inada T. Nascent peptide-dependent translation arrest leads to Not4p-mediated protein degradation by the proteasome. J Biol Chem. 2009;284(16):10343-52. Epub 2009/02/11. doi: 10.1074/jbc.M808840200. PubMed PMID: 19204001; PubMed Central PMCID: PMCPMC2667721.

50. Juszkiewicz S, Hegde RS. Quality Control of Orphaned Proteins. Mol Cell. 2018;71(3):443-57. Epub 2018/08/04. doi: 10.1016/j.molcel.2018.07.001. PubMed PMID: 30075143.

51. Brennan CM, Vaites LP, Wells JN, Santaguida S, Paulo JA, Storchova Z, et al. Protein aggregation mediates stoichiometry of protein complexes in aneuploid cells. Genes Dev. 2019. Epub 2019/06/15. doi: 10.1101/gad.327494.119. PubMed PMID: 31196865.

52. Osberg C, Aksnes H, Ninzima S, Marie M, Arnesen T. Microscopy-based Saccharomyces cerevisiae complementation model reveals functional conservation and redundancy of N-terminal acetyltransferases. Sci Rep. 2016;6:31627. Epub 2016/08/25. doi: 10.1038/srep31627. PubMed PMID: 27555049; PubMed Central PMCID: PMCPMC4995432.

53. Kim HK, Kim RR, Oh JH, Cho H, Varshavsky A, Hwang CS. The N-terminal

756 methionine of cellular proteins as a degradation signal. Cell. 2014;156(1-2):158-69.
757 Epub 2013/12/24. doi: 10.1016/j.cell.2013.11.031. PubMed PMID: 24361105;
758 PubMed Central PMCID: PMCPMC3988316.
759 54. Nguyen KT, Kim JM, Park SE, Hwang CS. N-terminal methionine excision of
760 proteins creates tertiary destabilizing N-degrons of the Arg/N-end rule pathway. J Biol
761 Chem. 2019;294(12):4464-76. Epub 2019/01/25. doi: 10.1074/jbc.RA118.006913.
762 PubMed PMID: 30674553; PubMed Central PMCID: PMCPMC6433082.
763 55. Lemieux B, Laterreur N, Perederina A, Noel JF, Dubois ML, Krasilnikov AS, et al.
764 Active Yeast Telomerase Shares Subunits with Ribonucleoproteins RNase P and
765 RNase MRP. Cell. 2016;165(5):1171-81. Epub 2016/05/10. doi:
766 10.1016/j.cell.2016.04.018. PubMed PMID: 27156450; PubMed Central PMCID:
767 PMCPMC4874874.
768 56. Diss G, Dube AK, Boutin J, Gagnon-Arsenault I, Landry CR. A systematic approach
769 for the genetic dissection of protein complexes in living cells. Cell Rep.
770 2013;3(6):2155-67. Epub 2013/06/12. doi: 10.1016/j.celrep.2013.05.004. PubMed
771 PMID: 23746448.
772 57. Diss G, Gagnon-Arsenault I, Dion-Cote AM, Vignaud H, Ascencio DI, Berger CM, et
773 al. Gene duplication can impart fragility, not robustness, in the yeast protein
774 interaction network. Science. 2017;355(6325):630-4. Epub 2017/02/12. doi:
775 10.1126/science.aai7685. PubMed PMID: 28183979.
776 58. Eisenberg AR, Higdon A, Keskin A, Hodapp S, Jovanovic M, Brar GA. Precise
777 Post-translational Tuning Occurs for Most Protein Complex Components during
778 Meiosis. Cell Rep. 2018;25(13):3603-17.e2. Epub 2018/12/28. doi:
779 10.1016/j.celrep.2018.12.008. PubMed PMID: 30590036.
780 59. Moriya H, Shimizu-Yoshida Y, Kitano H. In vivo robustness analysis of cell division
781 cycle genes in Saccharomyces cerevisiae. PLoS Genet. 2006;2(7):e111. Epub
782 2006/07/15. doi: 10.1371/journal.pgen.0020111. PubMed PMID: 16839182; PubMed
783 Central PMCID: PMCPMC1500812.